ACS OMEGA

http://pubs.acs.org/journal/acsodf

Article

Theoretical Study of ZnS Monolayer Adsorption Behavior for CO and HF Gas Molecules

Lalmuan Chhana, Bernard Lalroliana, Ramesh Chandra Tiwari, Bhanu Chettri, Lalrinthara Pachuau, Shivraj Gurung, Lalmuanpuia Vanchhawng, Dibya Prakash Rai, Lalhriat Zuala,* and Ramakrishna Madaka

Cite This: *ACS Omega* 2022, 7, 40176−40183

Read Online

ACCESS | Metrics & More | Article Recommendations

ABSTRACT: Adsorption of carbon monoxide (CO) and hydrogen fluoride (HF) gas molecules on a ZnS monolayer with weak van der Waals interactions is studied using the DFT + U method. From our calculation, the ZnS monolayer shows chemisorption with CO (E_{ads} = −0.96 eV) and HF (E_{ads} = −0.86 eV) gas molecules. Bader charge analysis shows that charge transfer is independent of the binding environment. A higher energy barrier for CO when migrating from one optimal site to another suggests that clustering may be avoided by the introduction of multiple CO molecules upon ZnS, while the diffusion energy barrier (DEB) for HF suggests that binding may occur more easily for HF gas upon the ZnS ML. Adsorption of the considered diatomic molecule also results in a significant variation in effective mass and therefore can be used to enhance the carrier mobility of the ZnS ML. Additionally, the calculation of recovery time shows that desirable sensing and desorption performance for CO and HF gas molecules can be achieved at room temperature (300 K).

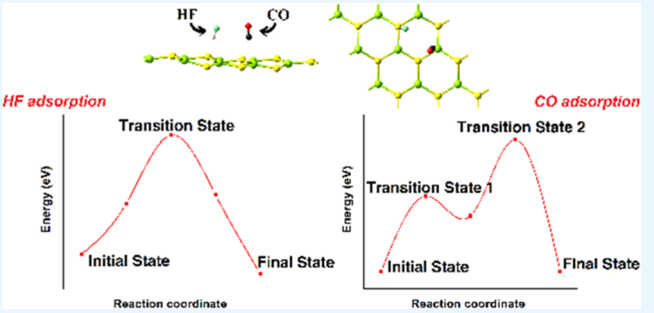

1. INTRODUCTION

In the atmosphere, carbon monoxide (CO) and hydrogen fluoride (HF) exist as colorless gases that can potentially cause significant changes in the environment as well as severe acute health effects.[1,2] Considering the growing interest in the environmental field and human health, efficient and effective sensing of these harmful gases is imperative. Therefore, attempts have been made to discover materials that possess promising sensing characteristics such as high selectivity, low noise, low power consumption, high recovery time, high limit of detection, low cost, and rapid response.[3,4] The discovery of low-dimensional graphitic structures[5] and their large surface area and high mobility of charge carriers increase the possibility of implementing them as a potential gas sensor.[6−8] However, due to the absence of band gap in graphene, various methods have been designed to improve its sensing ability,[9] including surface modification.[10,11] As a result, other graphene-like materials with a finite band gap, such as germanene,[12] MoS_2,[13] carbon nitride,[14] arsenene,[15] h-BN,[16] transition-metal dichalcogenides (TMDCs),[17,18] and many others were also studied extensively to explore their quality in gas sensing. Consequently, these two-dimensional (2D) materials are found to be highly suitable for gas sensing via modulating the carrier density and shifting the Fermi level.

After the stabilities and formation of 2D monolayers were verified experimentally,[19] the ZnS monolayer has attracted more attention due to its close morphologies with the ZnO monolayer,[20] which is known to possess interesting tunable properties in the field of nanoelectronics, including gas sensing.[21−23] Stabilities and promising tunable properties of ZnS have been studied extensively with respect to various applications.[24−29] With the ZnS nanowire already shown to possess promising properties in the field of sensing,[30] its monolayer counterpart may actually be far more promising due to the high surface−volume ratio as a result of its low-dimensional structure. Xu et al.,[31] in fact, demonstrated that the ZnS monolayer is a potential gas sensor for NH_3 gas with its high sensitivity and selectivity. However, a detailed study of ZnS sensing properties for harmful gases such as CO and HF is still not presented. Therefore, we hope to provide insight into the adsorption properties of ZnS through our theoretical study.

Received: August 8, 2022
Accepted: October 20, 2022
Published: October 28, 2022

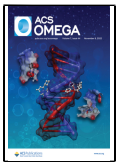

In this work, the interaction of CO and HF gas molecules with the ZnS monolayer (ZnS ML) is studied using first-principles calculations based on density functional theory with its van der Waals interactions corrected using DFT-D2 and its electronic interactions taken into account by introducing Hubbard potential (U) for strongly correlated orbitals. Geometry optimization and adsorption of CO/HF on the ZnS ML are first investigated to obtain the most stable configuration. Analysis of structures and electronic properties is done on the obtained most stable adsorbed configuration. Our results show that the ZnS monolayer exhibits chemisorption with both gas molecules. A higher energy barrier for CO suggests that clustering may be avoided by the introduction of multiple CO molecules upon ZnS, while the DEB for HF suggests that binding may occur more easily upon the ZnS ML in the case of HF adsorption. In addition to large adsorption energies, the calculation of recovery time shows that desirable sensing and desorption performance can be achieved at room temperature. The calculation of effective mass shows that the adsorption of both diatomic molecules results in a considerable variation in the effective mass and therefore can be used to enhance the carrier mobility of the ZnS ML.

2. COMPUTATIONAL DETAILS

Geometry optimizations and electronic property calculations were performed within the framework of spin-polarized plane-wave DFT as implemented in the Vienna Ab initio Simulation Package (VASP).[32] Generalized gradient approximation (GGA) as revised by Perdew, Burke, and Ernzerhof[33] was used for the plane-wave basis set in all relaxation processes. Projector augmented wave (PAW)[34] was used to describe the interactions between ions and electrons. For an accurate description of interactions between the monolayer and gas molecules, GGA-PBE and van der Waals were implemented in all of the calculations using DFT-D2 (Grimme).[35]

The orbital-dependent on-site Coulomb repulsion interactions between Zn:3d and S:3p electrons were taken into account using the DFT + U method. It is well known that the local density approximation (LDA) method overestimates the hybridization between Zn:3d orbitals. Also, DFT + U corrects self-interaction error (SIE), which is present not only in the d and f states but also in the s and p states.[36] Therefore, the Hubbard parameter, U, was added to the PBE functional to define the on-site Coulomb interaction in d orbitals[37] and also to correct SIE in the d and p orbitals.[38] We have adopted U parameters from Monteiro et al.[39] as U_{eff} (Zn:3d) = 14.36 eV and U_{eff} (S:3p) = 3.69 eV, which are obtained from the ACBN0 method, developed by Agapito et al.,[40] calculated directly from the Coulomb and exchange integrals.

A system of a 3 × 3 supercell is considered with 18 atoms consisting of nine Zn and O atoms each. A vacuum of 20 Å has been considered along the perpendicular Z-direction to avoid periodic interactions between the monolayers. All of the geometric structures are relaxed until the force on each atom is smaller than 0.005 eV/Å and by setting the energy convergence criteria of 10^{-6} eV. An energy cutoff of 400 eV is used for the plane-wave expansion of the electronic wave function, and the first Brillouin zone integration was performed using a 4 × 4 × 1 k-point mesh within the Monkhorst−Pack scheme.[41] For electronic structure calculations, the Brillouin zone is sampled by a denser 12 × 12 × 1 k-mesh.

The charge transfer between the ZnS ML and the adsorbed gas molecule is obtained via Bader charge analysis.[42] Adsorption energy (E_{ads}) is calculated to determine the strength of the adsorption process on the ZnS ML using the following equation

$$E_{\text{ads}} = E_{\text{total}} - (E_{\text{ZnS}} + E_{\text{gas molecule}}) \quad \text{(i)}$$

where E_{total}, E_{ZnS}, and $E_{\text{gas molecule}}$ are the total energy of the gas molecules adsorbed on the pristine ZnS monolayer, the pristine 3 × 3 supercell ZnS ML, and the isolated gas molecule, respectively.

Climbing image nudged elastic band (CI-NEB)[43] is used to calculate the transition state search (TSS). This method maps the minimum energy pathway between the initial and final configurations using a chain of configurations (images) connected by elastic springs. The diffusion energy barrier is then calculated from the following relation

$$E_{\text{DEB}} = E_{\text{TS}} - E_{\text{IS}} \quad \text{(ii)}$$

where E_{TS} and E_{IS} are the energies of the transition state and the initial state, respectively.

The recovery time for the gas molecules is estimated by the following equation

$$\tau = \upsilon_0^{-1}\, e^{-E_{\text{ads}}/kT} \quad \text{(iii)}$$

where υ_0 (= 10^{12} s^{-1})[44] is the attempted frequency of the molecule, E_{ads} is the adsorption energy, k (= 8.617 × 10^{-5} eV/K) is the Boltzmann constant, and T is the temperature.

For obtaining effective masses of electrons and holes, we used the parabolic E−k dispersion relation near the Γ-point in the form

$$E(k) = E_0 \pm \frac{\hbar^2 k^2}{2m^*_{\text{e,h}}} \quad \text{(iv)}$$

where E_0 is the energy eigenvalue of the selected conduction band minimum (CBM) or valence band maximum (VBM) used for the effective mass calculation and $m^*_{\text{e,h}}$ is the effective mass of electrons/holes.

Introduction of the gas molecules into the pristine ZnS ML induces changes in the conductivity of the system, which is calculated by the following relation

$$\sigma \propto \exp -(E_g/2kT) \quad \text{(v)}$$

where σ is the electrical conductivity of the material, k is the Boltzmann constant, T is the thermodynamic temperature, and E_g is the band gap energy.

Work function, defined as the minimum thermodynamic work (energy) required to remove an electron from the Fermi level to infinity, of the gas molecules before and after adsorption is also calculated using the equation

$$\Phi = V(\Phi) - E_{\text{Fermi}} \quad \text{(vi)}$$

where Φ, $V(\Phi)$, and E_{Fermi} are the work function, the electrostatic potential at the vacuum level, and the Fermi energy of the ZnS ML, respectively.

3. RESULTS AND DISCUSSION

To understand the optimal binding configuration of CO/HF molecules on the pristine ZnS ML, four adsorption sites are considered for each of CO and HF molecules upon the relaxed ZnS monolayer. The center of the ZnS hexagon is named as

https://doi.org/10.1021/acsomega.2c05064
ACS Omega 2022, 7, 40176−40183

site 1, the top of the Zn atom as site 2, the top of the S atom as site 3, and the site above the center of the Zn−S bond as site 4, as shown in Figure 1. For the adsorbed gas molecules on the

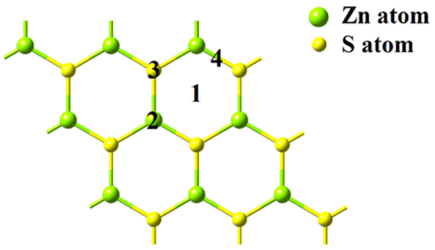

Figure 1. Adsorption sites of the gas molecules on the ZnS ML.

ZnS monolayer, the adsorption energy is calculated by the relation given in eq i. Our calculation shows that the adsorption energy for diatomic molecules (CO and HF) in the ZnS ML is the highest in site 1, i.e., the center of the ZnS hexagon. At site 1, the two diatomic molecules have two possible orientations, with either of the atoms in the gas molecule pointing to Zn or S atoms, which are all taken into consideration. However, regardless of the initial adsorption sites considered, all of the proposed sites result in the same configuration, as shown in Figure 2, after optimization. This may be the result of large minimization steps taken in each optimization. For proper convergence of the system with the input criteria and specific interaction of Zn-d and S-p orbitals, the minimization step limit is taken to a large value such that the diatomic molecules may have possibly shifted to the most optimal adsorption sites in each of the cases. Hence, the only optimal absorption site and its energy for CO and HF in that site, i.e., site 1, are given in Table 1. For optimal configurations, it can be seen that the adsorption of CO and HF molecules gives rise to structural deformations of the ZnS ML surface, as shown in Figure 2. In the case of the CO-ZnS system, the optimized structure shows that the CO molecule vertically aligns with the ZnS ML with the C atom toward the Zn atom (Figure 2a), with an adsorption energy of −0.96 eV. Similarly, HF aligns vertically toward the ZnS ML but with the H atom toward the S atom (Figure 2b), with a lower adsorption energy of −0.86 eV. The adsorption energies are both negative, indicating that the adsorption process is exothermic with a large adsorption distance of 2.55 and 2.57 Å for the CO-ZnS and HF-ZnS system, respectively. The observed results

Table 1. Optimized Geometric Parameters of CO and HF Adsorbed on Optimal Sites of ZnO-ML: Adsorption Energy (E_{ads}), Adsorption Distance of Nearest-Neighbor Atoms between the Gas Molecule and Substrate (h), Charge Transfer (Q) between the Gas Molecule and Substrate, and Diffusion Energy Barrier (DEB) upon the ZnS ML

gas molecule	adsorption sites	h (Å)	E_{ads} (eV)	Q (e)	DEB (eV)
CO	site 1 (C point Zn)	2.55	−0.96	0.02	1.89
HF	site 1 (H point S)	2.57	−0.86	−0.08	0.26

indicate that the two gas molecules show chemisorption on the pristine ZnS ML.

For further insight into the optimized configuration, a transition state search is performed between two optimal adsorption sites, as shown in Figure 3a,b, for CO and HF, respectively. The reaction path with respect to its energy shows that the optimal site taken for adsorption is, in fact, the lowest energy site, confirming the accuracy of adsorption energy calculations. In CO-ZnS, two transition states, TS1 and TS2, are observed, and TS2 is taken for DEB calculation. Consequently, the intermediate state is observed between TS1 and TS2. An intermediate is a short-lived unstable reaction in adsorption that is formed when migrating from the initial state toward the optimal final site. In this case, CO gas is shortly adsorbed by the S atom in-between the transition states. The diffusion energy barrier (DEB) is then calculated using the relation given in eq ii. The DEB for CO on the ZnS ML surface is found to be 1.89 eV, while HF shows a DEB of 0.26 eV. A higher energy barrier for CO when migrating from one optimal site to another suggests that clustering may be avoided by the introduction of multiple CO molecules upon ZnS. Meanwhile, the DEB for HF suggests that binding may occur more easily upon the ZnS ML in the case of HF adsorption, even without the application of external energy.

To understand the interaction between the gas molecules and ZnS ML, electronic band structures and DOS of the adsorbed systems are investigated. The electronic band structures of pristine ZnS ML and the adsorbed systems are shown in Figure 4. The band structure of the pristine ZnS ML shows a band gap of 3.34 eV (Figure 4a), which is consistent with previous DFT + U studies[39] and much larger than that obtained using GGA-PBE (2.54 eV). The presence of Fermi energy closer to the valence band maximum indicates p-type behavior. For CO- and HF-adsorbed ZnS ML systems, the conduction band numbers slightly increased, in comparison

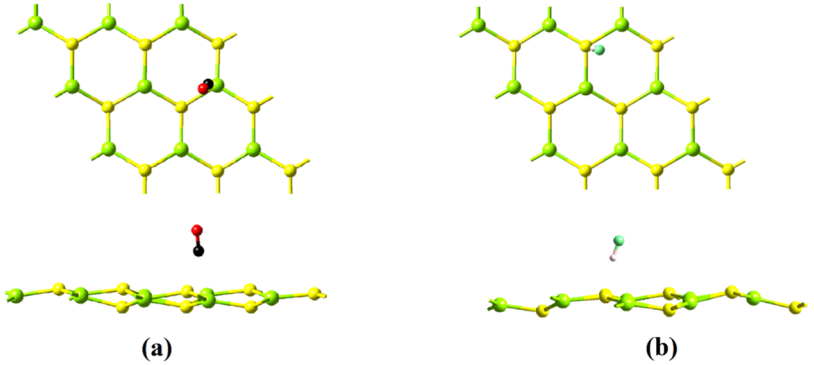

Figure 2. Most stable adsorption configurations (top and side view) of (a) CO and (b) HF adsorbed on the ZnS ML. The C, O, F, and H atoms are shown as black, red, cyan, and white balls, respectively.

https://doi.org/10.1021/acsomega.2c05064
ACS Omega 2022, 7, 40176−40183

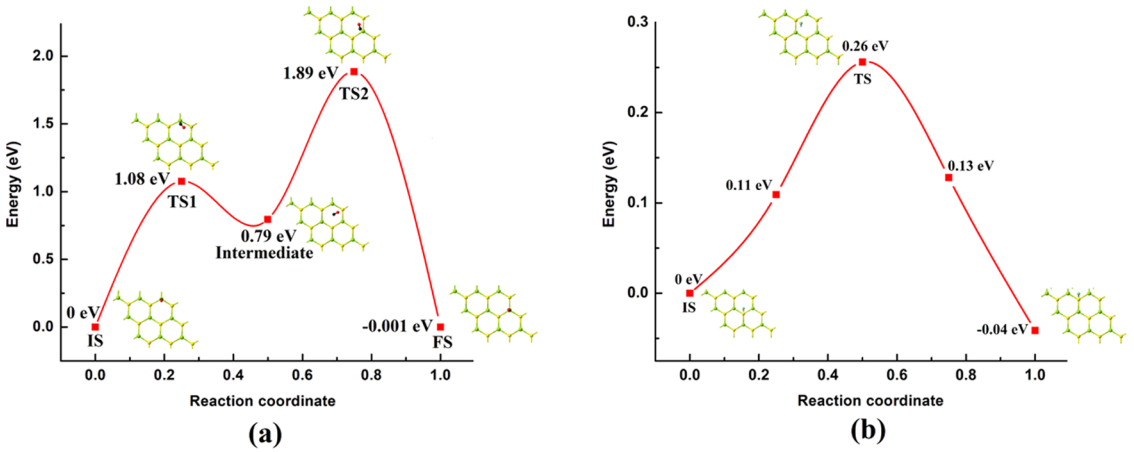

Figure 3. Diffusion energy barrier as a function of diffusion coordinate and diffusion pathway of (a) CO atoms and (b) HF atoms on the ZnS ML, where IS, TS, and FS are the initial state, transition state, and final state, respectively.

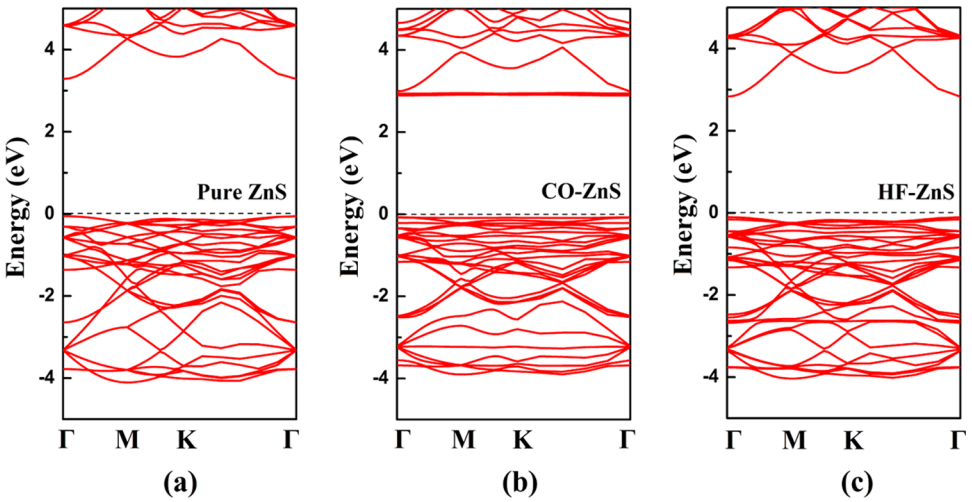

Figure 4. Band structures of (a) pristine ZnS ML, (b) CO-ZnS system, and (c) HF-ZnS system.

with the pristine system (Figure 4b,c). Both adsorbed systems also show a slight reduction in the energy band gap with a gap of 2.96 and 2.94 eV for the CO- and HF-adsorbed systems, respectively, as shown in Table 2. Our calculation shows that the ZnS ML exhibits nonmagnetic semiconductor properties before and after adsorption of the proposed gas molecules.

For analysis of the new band lines and contribution of the gas molecules in adsorbed ZnS ML, we calculate the total density of states (TDOS) and projected density of states (PDOS) for the pristine and the adsorbed systems. Figure 5 shows the resultant DOS of pristine ZnS ML and CO-ZnS and HF-ZnS systems. In contrast to the pristine ZnS ML, the CO-ZnS system shows new peaks around 3 eV, which is attributed to C 2p and O 2p orbitals. In the case of the HF-ZnS system, a new peak is observed at around −2.5 eV due to the F 2p orbitals. In all of the systems, the filled valence bands near the Fermi level are mostly the bonding states of d orbitals of Zn and p orbitals of S. On the other hand, the bottom of the conduction band is formed mainly by the unoccupied s and d orbitals of Zn and empty p orbitals of S in the case of the pristine system.

Table 2. Band Gap Energy (E_g), Effective Mass, and Work Function (Φ) of Pristine and Gas-Adsorbed ZnS ML

		effective mass (× m_e)			
system	band gap E_g (eV)	m_e^*	m_{hh}^*	m_{lh}^*	work function Φ (eV)
Pristine ZnS ML	3.34	0.18 0.24[a] (ZB) 0.30[a] (WZ) 0.28[b]	1.67 0.86[a]	1.003 0.18[a]	6.001
CO-ZnS	2.96	3.39	2.78	2.03	6.104
HF-ZnS	2.94	0.23	2.79	2.12	6.402

[a]Ref. D'Amico et al.[47] (bulk ZnS structure). [b]Ref. Miklosz et al.[48] (experimental value of bulk ZnS).

In gas sensors, recovery time can be used to calculate reusability. Using the relation given in eq iv, the recovery time of the two gas molecules was calculated at different temperatures and is plotted in Figure 6. We have found that at room temperature, the recovery time of CO upon ZnS ML was 1.34×10^4 s (~3.73 h), and HF molecules exhibit a further rapid recovery time of 2.81×10^2 s (~4.68 min), which shows that desirable sensing with rapid recovery time can be achieved for both gas molecules at an ambient temperature (300 K).[45,46] Recovery time was further studied to see the variation under different temperatures (at T = 200 and 400 K). At 200 K, CO

https://doi.org/10.1021/acsomega.2c05064
ACS Omega 2022, 7, 40176−40183

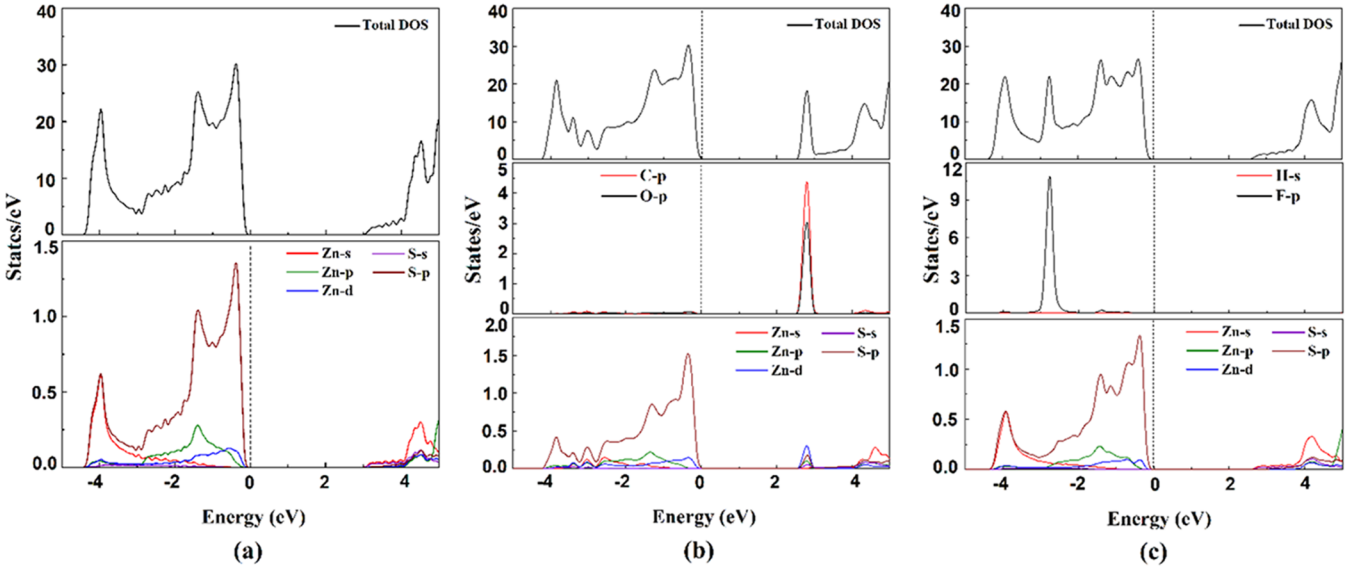

Figure 5. Projected density of states (PDOS) of (a) pristine ZnS ML, (b) CO-ZnS system, and (c) HF-ZnS system.

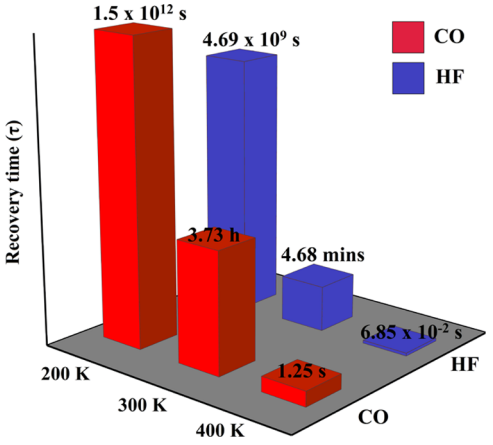

Figure 6. Recovery time of the ZnS monolayer for CO/HF gas desorption.

and HF showed recovery times of 1.5×10^{12} and 4.69×10^{9} s, respectively. Meanwhile, at an elevated temperature of 400 K, CO and HF showed recovery times of 1.25 and 6.85×10^{-2} s, respectively. Decreasing the temperature results in a longer recovery time, which may be too large, while an increase in the temperature decreases its recovery time by a considerable range. Nonetheless, this observation shows that the desirable sensing and reusability of ZnS ML for CO and HF can be achieved effectively at room temperature.

For the relaxed ZnS monolayer, the effective mass of electron m_e^* is calculated to be 0.18 m_e, which is slightly smaller than the reported value of 0.24 m_e and 0.30 m_e for zinc blende (ZB) and wurtzite (WZ) structures, respectively,[47] and an experimental value of 0.28 m_e.[48] Effective mass of light holes and heavy holes are found to be 1.003 m_e and 1.67 m_e, respectively, which is significantly larger than that of its zinc blende structure counterpart of 0.18 m_e and 0.86 m_e, respectively. Differences in the value of effective mass from its bulk counterpart may be attributed to the deviation of its band structure from the parabolic E vs k^2 relation.[49] In the direction considered within the reciprocal space, VBM shows slightly flat band lines (shown in Figure 4a) in comparison with its bulk counterpart. This is attributed to the variation in the effective mass of holes in the monolayer structure. With the adsorption of CO, the effective mass significantly increases to values of 3.39 m_e, 2.03 m_e, and 2.78 m_e for electrons, light holes, and heavy holes, respectively. These changes in the electron effective mass are also evident from the changes in the curvature around the band edge in the electronic band structure, particularly on the significantly visible flat band lines of the CBM. In this case of flat band lines, electron effective mass should be large according to the electronic band theory, which is consistent with our finding. Meanwhile, in addition to reducing its band gap energy, the adsorption of HF molecules does not offer significant changes in the conduction band nature of the pristine ZnS. This, in fact, is reflected upon its electron effective mass, which is found to be 0.23 m_e. The effective mass of light holes and heavy holes, however, are significantly increased to 2.12 m_e and 2.79 m_e, respectively, which is evident from its VBM along the reciprocal space (Figure 4c). Significant variations in the hole effective mass are observed both in the case of CO and HF adsorption, which could be quite promising for modifying its carrier mobility. In the case of electron effective mass variation, CO adsorption particularly yields a very interesting result owing to its nonisolated flat band line in the CBM. This flat band line indicates a type of band structure with constant energy independent of the crystal momentum. Apart from its enhanced carrier mobility, this particular nature is known to have potential in the study of superconductivity.[50,51]

Bader charge analysis from electronic charge calculation shows charge transfer between HF and ZnS ML ($\sim -0.08e$) to be significantly larger in comparison with the CO/ZnS ML system ($\sim 0.02e$). Test calculation shows that the charge transfer between these gas molecules and ZnS ML remains the same with or without the introduction of the Hubbard parameter. This observation shows that charge transfer depends on the universal properties of the gas molecules and 2D materials rather than the local binding environments, which is consistent with previous studies on these particular charge transfer characteristics.[52] For a better understanding of charge transfer, the electronic charge density difference for the CO-ZnS and HF-ZnS system is calculated, as shown in Figure 7.

https://doi.org/10.1021/acsomega.2c05064
ACS Omega 2022, 7, 40176−40183

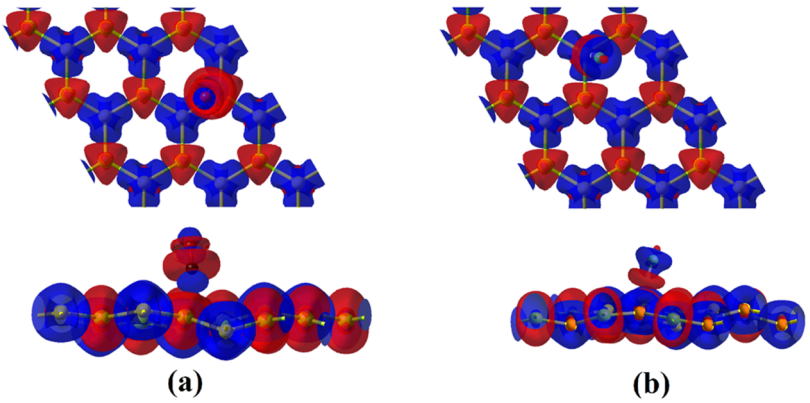

Figure 7. Total charge densities of (a) CO-ZnS and (b) HF-ZnS systems at an isosurface value of 0.02 eV/Å^3.

Blue and red colors represent charge depletion and accumulation at an isovalue of 0.02 eV/Å^3, respectively. It is indicated in the figure that there is a charge accumulation on the pristine ZnS surface for CO gas molecules, suggesting the charge-donor characteristics. On the other hand, HF acts as an electron acceptor and accepts electrons from pristine ZnS as observed from the charge density difference plot. The observation is in agreement with the charge transfer from Bader charge analysis. Charge transfer when exposed to gases has a key effect on the resistance. Charge depletion reduces charge carriers in the monolayer and enhances its resistance, while accumulation increases charge carriers and results in the reduction of its resistance.

Furthermore, the change in conductivity due to the variation in carrier mobility after the adsorption of CO/HF gas is further analyzed using eq v. The equation indicates that the conductivity is proportional to the exponential of band gap, which reflects that a change in the band gap width results in a change in the conductivity. Our calculation shows that the adsorption of both gas molecules results in a change in the band gap energy, i.e., 0.38 and 0.40 eV for CO and HF/ZnS systems, respectively. Although the energy change in the gap may seem small, its exponential value can result in significant variations at different temperatures. This suggests that the adsorption of CO/HF gas molecules possesses the possibility of modifying the conductivity of ZnS ML, as observed earlier from effective mass calculations.

Work function, which is equal to the potential difference between the Fermi energy and the electrostatic potential outside the system, is also calculated from the relation given in eq vi. In comparison with the pristine ZnS ML (6.001 eV), the work function after chemisorption of CO and HF becomes 6.104 and 6.402 eV, respectively, as shown in Table 2. When adsorption occurs, charge concentration changes in both the gas molecules and the substrate, which alters the conductivity of the surface. This is closely related to the work function of the surface.[53] As discussed earlier in Bader charge analysis, charge transfer and its alteration of work function are independent of the local binding environment but rather depend on the nature of elements. Hence, a slightly larger variation in work function is observed in HF adsorption, although CO offers larger adsorption energy. Nonetheless, this alteration of the work function of the ZnS ML upon gas adsorption thereby confirms the presence of strong interactions between the two systems. This variation also indicates that two gases can be distinguished via measuring the work function.

4. CONCLUSIONS

Our DFT + U calculations show that the ZnS monolayer shows high adsorption energies for CO and HF gas molecules. The calculated adsorption energies are −0.96 and −0.86 eV for CO and HF gas, respectively. The higher energy barrier for CO when migrating from one optimal site to another suggests that clustering may be avoided by the introduction of multiple CO molecules upon ZnS, while the DEB for HF suggests that binding may occur more easily for HF gas upon the ZnS ML. Calculation of recovery time shows that desirable sensing and desorption performance for CO and HF gas molecules can be achieved at 300 K. Changes in effective mass with the adsorption of these gas molecules open the possibility of tuning carrier mobility and hence the electrical property of two-dimensional ZnS structure. Bader charge analysis shows that charge transfer is independent of the binding environment. Our calculations indicate that chemisorption also results in the shift of work function, further confirming the strong interaction between the gas molecules and the substrate. From our study, we hope to provide insight into the sensing property of ZnS ML and the possibility of tuning such property through effective means in future studies.

AUTHOR INFORMATION

Corresponding Author

Lalhriat Zuala − *Physical Sciences Research Centre (PSRC), Pachhunga University College, Mizoram University, Aizawl 796001 Mizoram, India;* orcid.org/0000-0003-3946-7292; Email: hriatamail@gmail.com

Authors

Lalmuan Chhana − *Department of Physics, School of Physical Sciences, Mizoram University, Aizawl 796004 Mizoram, India; Physical Sciences Research Centre (PSRC), Pachhunga University College, Mizoram University, Aizawl 796001 Mizoram, India*

Bernard Lalroliana − *Department of Physics, School of Physical Sciences, Mizoram University, Aizawl 796004 Mizoram, India; Physical Sciences Research Centre (PSRC), Pachhunga University College, Mizoram University, Aizawl 796001 Mizoram, India*

Ramesh Chandra Tiwari − *Department of Physics, School of Physical Sciences, Mizoram University, Aizawl 796004 Mizoram, India*

Bhanu Chettri − *North Eastern Hill University, Shillong 793022 Meghalaya, India; Physical Sciences Research Centre*

https://doi.org/10.1021/acsomega.2c05064
ACS Omega 2022, 7, 40176−40183

(PSRC), Pachhunga University College, Mizoram University, Aizawl 796001 Mizoram, India

Lalrinthara Pachuau − *Physical Sciences Research Centre (PSRC), Pachhunga University College, Mizoram University, Aizawl 796001 Mizoram, India*

Shivraj Gurung − *Physical Sciences Research Centre (PSRC), Pachhunga University College, Mizoram University, Aizawl 796001 Mizoram, India*

Lalmuanpuia Vanchhawng − *Physical Sciences Research Centre (PSRC), Pachhunga University College, Mizoram University, Aizawl 796001 Mizoram, India*

Dibya Prakash Rai − *Physical Sciences Research Centre (PSRC), Pachhunga University College, Mizoram University, Aizawl 796001 Mizoram, India;* orcid.org/0000-0002-3803-8923

Ramakrishna Madaka − *Department of Physics, Indian Institute of Technology Madras, Chennai 600036 Tamil Nadu, India*

Complete contact information is available at: https://pubs.acs.org/10.1021/acsomega.2c05064

Notes

The authors declare no competing financial interest.

■ ACKNOWLEDGMENTS

Financial support for this research work was provided by SERB-DST, Govt. of India, vide Grant No. EEQ/2018/000854 dated 23rd May 2019 as Major Research Project.

■ REFERENCES

(1) Cho, S.-Y.; Woo, K.-H.; Kim, J.-S.; Yoon, S.-Y.; Na, J.-Y.; Yu, J.-H.; Kim, Y.-B. Acute Symptoms in Firefighters who Participated in Collection Work after the Community Hydrogen Fluoride Spill Accident. *Ann. Occup. Environ. Med.* **2013**, *25*, No. 36.

(2) Kuhns, H. D.; Mazzoleni, C.; Moosmüller, H.; Nikolic, D.; Keislar, R. E.; Barber, P. W.; Li, Z.; Etyemezian, V.; Watson, J. G. Remote sensing of PM, NO, CO and HC emission factors for on-road gasoline and diesel engine vehicles in Las Vegas, NV. *Sci. Total Environ.* **2004**, *322*, 123−137.

(3) Kourosh Kalantar-zadeh, B. F.*Nanotechnology-Enabled Sensors*; Springer, 2008.

(4) Basu, S.; Bhattacharyya, P. Recent developments on graphene and graphene oxide based solid state gas sensors. *Sens. Actuators, B* **2012**, *173*, 1−21.

(5) Novoselov, K. S.; Geim, A. K.; Morozov, S. V.; Jiang, D.; Katsnelson, M. I.; Grigorieva, I. V.; Dubonos, S. V.; Firsov, A. A. Two-dimensional gas of massless Dirac fermions in graphene. *Nature* **2005**, *438*, 197−200.

(6) Varghese, S. S.; Varghese, S. H.; Swaminathan, S.; Singh, K.; Mittal, V. J. E. Two-Dimensional Materials for Sensing: Graphene and Beyond. *Electronics* **2015**, *4*, 651−687.

(7) Chen, G.; Paronyan, T. M.; Harutyunyan, A. R. Sub-ppt gas detection with pristine graphene. *Appl. Phys. Lett.* **2012**, *101*, No. 053119.

(8) Schedin, F.; Geim, A. K.; Morozov, S. V.; Hill, E. W.; Blake, P.; Katsnelson, M. I.; Novoselov, K. S. Detection of individual gas molecules adsorbed on graphene. *Nat. Mater.* **2007**, *6*, 652−655.

(9) Yu, L.; Li, F. Metal dimers embedded vertically in defect-graphene as gas sensors: a first-principles study. *Phys. Chem. Chem. Phys.* **2022**, *24*, 9842−9847.

(10) Robinson, J. T.; Perkins, F. K.; Snow, E. S.; Wei, Z.; Sheehan, P. E. Reduced Graphene Oxide Molecular Sensors. *Nano Lett.* **2008**, *8*, 3137−3140.

(11) Lu, G.; Ocola, L. E.; Chen, J. Reduced graphene oxide for room-temperature gas sensors. *Nanotechnology* **2009**, *20*, No. 445502.

(12) Xia, W.; Hu, W.; Li, Z.; Yang, J. A first-principles study of gas adsorption on germanene. *Phys. Chem. Chem. Phys.* **2014**, *16*, 22495−22498.

(13) Late, D. J.; Huang, Y. K.; Liu, B.; Acharya, J.; Shirodkar, S. N.; Luo, J.; Yan, A.; Charles, D.; Waghmare, U. V.; Dravid, V. P.; Rao, C. N. Sensing behavior of atomically thin-layered MoS2 transistors. *ACS Nano* **2013**, *7*, 4879−4891.

(14) Bhattacharyya, K.; Pratik, S. M.; Datta, A. Controlled Pore Sizes in Monolayer C2N Act as Ultrasensitive Probes for Detection of Gaseous Pollutants (HF, HCN, and H2S). *J. Phys. Chem. C* **2018**, *122*, 2248−2258.

(15) Kamal, C.; Ezawa, M. Arsenene: Two-dimensional buckled and puckered honeycomb arsenic systems. *Phys. Rev. B* **2015**, *91*, No. 085423.

(16) Chettri, B.; Patra, P. K.; Hieu, N. N.; Rai, D. P. Hexagonal boron nitride (h-BN) nanosheet as a potential hydrogen adsorption material: A density functional theory (DFT) study. *Surf. Interfaces* **2021**, *24*, No. 101043.

(17) Wang, Q. H.; Kalantar-Zadeh, K.; Kis, A.; Coleman, J. N.; Strano, M. S. Electronics and optoelectronics of two-dimensional transition metal dichalcogenides. *Nat. Nanotechnol.* **2012**, *7*, 699−712.

(18) Guo, H.; Zheng, K.; Cui, H.; Zhang, F.; Yu, J.; Tao, L.-Q.; Li, X.; Chen, X. High sensitivity gas sensor to detect SF6 decomposition components based on monolayer antimonide phosphorus. *Chem. Phys. Lett.* **2020**, *756*, No. 137868.

(19) Ivanovskii, A. L. Graphene-based and graphene-like materials. *Russ. Chem. Rev.* **2012**, *81*, 571−605.

(20) Fang, X. S.; Zhang, L. D. Controlled growth of one-dimensional oxide nanomaterials. *J. Mater. Sci. Technol.* **2006**, *22*, 1−18.

(21) Chen, H.; Qu, Y.; Ding, J.; Fu, H. Adsorption behavior of graphene-like ZnO monolayer with oxygen vacancy defects for NO2: A DFT study. *Superlattices Microstruct.* **2019**, *134*, No. 106223.

(22) Lei, J.; Xu, M.-C.; Hu, S.-J. Anchoring transition metal elements on graphene-like ZnO monolayer by CO molecule to obtain spin gapless semiconductor. *Appl. Surf. Sci.* **2017**, *416*, 681−685.

(23) Zhang, Y.-H.; Zhang, M.-L.; Zhou, Y.-C.; Zhao, J.-H.; Fang, S.-M.; Li, F. Tunable electronic and magnetic properties of graphene-like ZnO monolayer upon doping and CO adsorption: a first-principles study. *J. Mater. Chem. A* **2014**, *2*, 13129−13135.

(24) Chhana, L.; Tiwari, R. C.; Chettri, B.; Rai, D. P.; Gurung, S.; Zuala, L. Ab initio investigation of non-metal-doped ZnS monolayer. *Appl. Phys. A* **2021**, *127*, 729.

(25) Rai, D. P.; Kaur, S.; Srivastava, S. Band gap modulation of mono and bi-layer hexagonal ZnS under transverse electric field and bi-axial strain: A first principles study. *Phys. B* **2018**, *531*, 90−94.

(26) Lashgari, H.; Boochani, A.; Shekaari, A.; Solaymani, S.; Sartipi, E.; Mendi, R. T. Electronic and optical properties of 2D graphene-like ZnS: DFT calculations. *Appl. Surf. Sci.* **2016**, *369*, 76−81.

(27) Es-Smairi, A.; Fazouan, N.; Atmani, E. H. Enhanced optical and thermoelectric properties of ZnS monolayer and stacked bilayer compared with bulk. *Mater. Res. Express* **2019**, *6*, No. 125047.

(28) Peng, Q.; Han, L.; Wen, X.; Liu, S.; Chen, Z.; Lian, J.; De, S. Mechanical properties and stabilities of g-ZnS monolayers. *RSC Adv.* **2015**, *5*, 11240−11247.

(29) Behera, H.; Mukhopadhyay, G. Tailoring the structural and electronic properties of a graphene-like ZnS monolayer using biaxial strain. *J. Phys. D: Appl. Phys.* **2014**, *47*, No. 075302.

(30) Wang, X.; Xie, Z.; Huang, H.; Liu, Z.; Chen, D.; Shen, G. Gas sensors, thermistor and photodetector based on ZnS nanowires. *J. Mater. Chem.* **2012**, *22*, 6845−6850.

(31) Xu, Y.; Meng, R.; Xiong, D.; Sun, X.; Wang, S.; Xiao, J.; Chen, X. Monolayer ZnS as a Promising Candidate for NH3 Sensor: A First-Principle Study. *IEEE Sens. J.* **2017**, *17*, 6515−6521.

(32) Kresse, G.; Furthmüller, J. Efficient iterative schemes for ab initio total-energy calculations using a plane-wave basis set. *Phys. Rev. B* **1996**, *54*, 11169−11186.

(33) Perdew, J. P.; Burke, K.; Ernzerhof, M. Generalized Gradient Approximation Made Simple. *Phys. Rev. Lett.* **1996**, *77*, 3865−3868.

(34) Blöchl, P. E. Projector augmented-wave method. *Phys. Rev. B* **1994**, *50*, 17953−17979.
(35) Grimme, S. Semiempirical GGA-type density functional constructed with a long-range dispersion correction. *J. Comput. Chem.* **2006**, *27*, 1787−1799.
(36) Kulik, H. J.; Cococcioni, M.; Scherlis, D. A.; Marzari, N. Density Functional Theory in Transition-Metal Chemistry: A Self-Consistent Hubbard U Approach. *Phys. Rev. Lett.* **2006**, *97*, No. 103001.
(37) Dudarev, S. L.; Botton, G. A.; Savrasov, S. Y.; Humphreys, C. J.; Sutton, A. P. Electron-energy-loss spectra and the structural stability of nickel oxide: An LSDA+U study. *Phys. Rev. B* **1998**, *57*, 1505−1509.
(38) Kulik, H. J.; Marzari, N. A self-consistent Hubbard U density-functional theory approach to the addition-elimination reactions of hydrocarbons on bare FeO+. *J. Chem. Phys.* **2008**, *129*, No. 134314.
(39) Monteiro, J. R. M.; Mota, C.; Gusmão, M. S. S.; Ghosh, A.; Frota, H. O. Mechanical and dynamic stability of ZnX chalcogenide (X = O, S, Se, Te) monolayers and their electronic, optical, and thermoelectric properties. *J. Appl. Phys.* **2021**, *130*, No. 045110.
(40) Agapito, L. A.; Curtarolo, S.; Buongiorno Nardelli, M. Reformulation of $\mathrm{DFT}+U$ as a Pseudohybrid Hubbard Density Functional for Accelerated Materials Discovery. *Phys. Rev. X* **2015**, *5*, No. 011006.
(41) Monkhorst, H. J.; Pack, J. D. Special points for Brillouin-zone integrations. *Phys. Rev. B* **1976**, *13*, 5188−5192.
(42) Henkelman, G.; Arnaldsson, A.; Jónsson, H. A fast and robust algorithm for Bader decomposition of charge density. *Comput. Mater. Sci.* **2006**, *36*, 354−360.
(43) Henkelman, G.; Uberuaga, B. P.; Jónsson, H. A climbing image nudged elastic band method for finding saddle points and minimum energy paths. *J. Chem. Phys.* **2000**, *113*, 9901−9904.
(44) Peng, S.; Cho, K.; Qi, P.; Dai, H. Ab initio study of CNT NO2 gas sensor. *Chem. Phys. Lett.* **2004**, *387*, 271−276.
(45) Zhao, Z.; Yong, Y.; Zhou, Q.; Kuang, Y.; Li, X. Gas-Sensing Properties of the SiC Monolayer and Bilayer: A Density Functional Theory Study. *ACS Omega* **2020**, *5*, 12364−12373.
(46) Liu, T.; Cui, Z.; Li, X.; Cui, H.; Liu, Y. Al-Doped MoSe2 Monolayer as a Promising Biosensor for Exhaled Breath Analysis: A DFT Study. *ACS Omega* **2021**, *6*, 988−995.
(47) D'Amico, P.; Calzolari, A.; Ruini, A.; Catellani, A. New energy with ZnS: novel applications for a standard transparent compound. *Sci. Rep.* **2017**, *7*, No. 16805.
(48) Miklosz, J. C.; Wheeler, R. G. Exciton Structure and Magneto-Optical Effects in ZnS. *Phys. Rev.* **1967**, *153*, 913−923.
(49) Agasiev, A. A.; Muradov, M. B. Formation of cadmium sulfide particles in the bulk of the polymer matrix. *Pisma Zh. Technicheskoy Fiz.* **1991**, *17*, 54.
(50) Huhtinen, K.-E.; Herzog-Arbeitman, J.; Chew, A.; Bernevig, B. A.; Törmä, P. Revisiting flat band superconductivity: Dependence on minimal quantum metric and band touchings. *Phys. Rev. B* **2022**, *106*, No. 014518.
(51) Volovik, G. E. Graphite, Graphene, and the Flat Band Superconductivity. *JETP Lett.* **2018**, *107*, 516−517.
(52) Hou, R.; Xia, Y.; Yang, S. A Linear Relationship between the Charge Transfer Amount and Level Alignment in Molecule/Two-Dimensional Adsorption Systems. *ACS Omega* **2020**, *5*, 26748−26754.
(53) Barsan, N.; Koziej, D.; Weimar, U. Metal oxide-based gas sensor research: How to? *Sens. Actuators, B* **2007**, *121*, 18−35.

https://doi.org/10.1021/acsomega.2c05064
ACS Omega 2022, 7, 40176−40183